Conformational Changes of the 120-kDa Na + /Ca 2+ Exchanger Protein upon Ligand Binding: A Fourier Transform Infrared Spectroscopy Study †

ARTICLE *in* ANNALS OF THE NEW YORK ACADEMY OF SCIENCES · DECEMBER 2002

Impact Factor: 4.38 · DOI: 10.1021/bi0010672 · Source: PubMed

4 AUTHORS, INCLUDING:

Erik Goormaghtigh
Université Libre de Bruxelles
170 PUBLICATIONS **5,721** CITATIONS

SEE PROFILE

Jean-Marie Ruysschaert
Université Libre de Bruxelles
472 PUBLICATIONS **13,955** CITATIONS

SEE PROFILE

Andre Herchuelz
Université Libre de Bruxelles
155 PUBLICATIONS **4,203** CITATIONS

SEE PROFILE

Conformational Changes of the 120-kDa Na^+/Ca^{2+} Exchanger Protein upon Ligand Binding: A Fourier Transform Infrared Spectroscopy Study†

Rami I. Saba,*,‡,§ Erik Goormaghtigh,|| Jean-Marie Ruysschaert,|| and André Herchuelz‡

Laboratoire de Pharmacodynamie et de Thérapeutique, Faculté de Médecine, Bât. GE, 808 route de Lennik, B-1070, Brussels, Belgium, and Laboratoire de Chimie Physique des Macromolecules aux Interfaces, Faculté de Sciences, Campus Plaine, Boulevard du Triomphe, Université Libre de Bruxelles, B-1050, Brussels, Belgium

Received May 10, 2000; Revised Manuscript Received January 9, 2001

ABSTRACT: The 120-kDa Na^+/Ca^{2+} exchanger was purified and reconstituted into lipid vesicles. The secondary structure composition of the exchanger was 39% α-helices, 20% β-sheets, 25% β-turns, and 16% random coils, as analyzed by Fourier transform infrared attenuated total reflection spectroscopy. The secondary structure composition of the COOH-terminal portion of the *protein* was compatible with a topology model containing 4−6 transmembrane segments. Furthermore, the secondary structure of the NH_2-terminal portion of the *cytoplasmic loop* was analyzed and found to be different from that of the COOH-terminal portion. Ca^{2+} and/or the exchange inhibitory peptide (XIP) failed to affect the secondary structure of the 120-kDa protein. Tertiary structure modifications induced by Ca^{2+} and XIP were analyzed by monitoring the hydrogen/deuterium exchange rate for the reconstituted exchanger. In the absence of ligand, 51% of the protein was accessible to solvent. Ca^{2+} decreased accessibility to 40%, implicating the shielding of at least 103 amino acids. When both Ca^{2+} and XIP were added, accessibility increased to 66%. No modification was obtained when XIP was added alone. Likewise, in the presence of Ca^{2+}, XIP failed to modify the tertiary structure of the 70-kDa protein, suggesting that XIP acts at the level of the COOH-terminal portion of the intracellular loop. The present data describe, for the first time, conformational changes of the Na^+/Ca^{2+} exchanger induced by Ca^{2+} and XIP, compatible with an interaction model where regulatory Ca^{2+} and inhibitory XIP bind to distinct sites, and where XIP binding requires the presence of Ca^{2+}.

In cardiac myocytes, changes in the cytosolic free Ca^{2+} concentration play a major role in the process of excitation−contraction coupling (*1*, *2*). Hence, the cytosolic free Ca^{2+} concentration must be tightly controlled. In the heart, the major process mediating Ca^{2+} extrusion from myocytes occurs via the Na^+/Ca^{2+} exchanger protein (*3*, *4*). The Na^+/Ca^{2+} exchanger is an electrogenic transporter coupling Na^+ and Ca^{2+} counter-transport with a stoichiometry of 3 Na^+ for 1 Ca^{2+} (*5*). The Na^+/Ca^{2+} exchange mechanism is most probably a consecutive one where Na^+ and Ca^{2+} are transported in separate steps involving two major conformational changes (E_1 and E_2) (*6*−*8*). Moreover, the temperature-dependence curve of Na^+/Ca^{2+} exchange implies that at least two reactions and three intermediate conformations are involved in Ca^{2+} transport (*9*, *10*).

The exchanger protein was successfully purified and reconstituted (*11*−*13*), and the Na^+/Ca^{2+} exchanger has been cloned from various tissues (*14*−*17*). The hydropathy profile predicts 11 transmembrane segments, 5 downstream and 6 upstream of a large hydrophilic cytoplasmic loop (*14*, *18*). However, recent mutational studies suggest that the topology of the exchanger could be slightly different (*19*, *20*). The native Na/Ca exchanger protein has a theoretical molecular mass of 110 kDa, based on amino acid sequence determination (*14*). Electrophoresis gels show two protein bands at 160 and 120 kDa under nonreducing conditions. Reducing agents decrease the intensity of the 160-kDa band and lead to the appearance of a 70-kDa protein band (*11*). It is currently accepted that the 120-kDa band represents the native protein, the 70-kDa band being a proteolysis fragment of the native protein (*11*, *12*), and the 160-kDa band an alternate form of the 120-kDa protein (*11*, *12*). Thus, while the 120- and 160-kDa proteins are immunologically related and have the same NH_2-terminus, the 160-kDa protein is only seen under nonreducing conditions, indicating that both proteins are identical but differ only in their migration profile on SDS−PAGE[1] gels (*11*−*13*).

Two of the most important activity regulators of the exchanger are Ca^{2+} and an endogenous calmodulin-like

† This study was supported by the Belgian Fund for Scientific Research (FRSM 3.4545.96, LN 9.4514.93, and LN 9.4510.95).

* Corresponding author.

‡ Laboratoire de Pharmacodynamie et de Thérapeutique, Université Libre de Bruxelles.

§ Present address: CWRU SOM W-353, YANG Laboratory, 2109 Adelbert Rd., Cleveland, OH 44106-4965. Tel: (216) 368 5164. Fax: (216) 368-3395. E-mail: rxs138@po.cwru.edu.

|| Laboratoire de Chimie Physique des Macromolecules aux Interfaces.

[1] Abbreviations: aas, amino acids; Ca_o, extracellular calcium ions; FTIR-ATR, Fourier transform infrared attenuated total reflection; H/D, hydrogen/deuterium; MOPS, 4-morpholinepropanesulfonic acid; Na_i, intracellular sodium ions; NCX, sodium/calcium exchanger; NEM, *N*-ethylmaleimide; PAGE, polyacrylamide gel electrophoresis; SLVs, sarcolemmal vesicles; SNA, sulfosuccinimidyl acetate; Tris, 2-amino-2-(hydroxymethyl)-1,3-propanediol; XIP, exchanger inhibitory peptide.

10.1021/bi0010672 CCC: $20.00
Published on Web 02/20/2001

binding region of the exchanger. Thus, the exchanger activity is inhibited in the absence of Ca^{2+} (*21*, *22*), and the high-affinity Ca^{2+} binding site, different from the site of Ca^{2+} transport, of the cardiac exchanger has been located at the level of the large cytoplasmic loop (*23*, *24*). Moreover, the mobility of the Na/Ca exchanger protein increases during SDS−PAGE when Ca^{2+} is present in the gel loading buffer, indicating that Ca^{2+} binding to the protein induces conformational changes (*24*). Furthermore, the beginning of the large cytoplasmic loop contains a sequence rich in basic and hydrophobic amino acid residues (aas) that is homologous to a calmodulin binding domain (*25*). A synthetic peptide of 20 aas, termed XIP, identical in sequence to that region, inhibits Na^+/Ca^{2+} exchange activity in several cellular preparations (*25*−*27*).

Until now, the conformational changes induced by regulatory Ca^{2+} and/or XIP binding have not been characterized at the molecular level. Such a characterization will provide a better understanding of the activation or inhibition mechanisms of Ca^{2+} and XIP, respectively, in relation to the conformational changes induced by these ligands. In the present study, we have determined the secondary structure of the purified and reconstituted active 120-kDa Na^+/Ca^{2+} exchanger by FTIR-ATR spectroscopy. Moreover, modifications of the tertiary structure, induced by Ca^{2+} and/or XIP, were investigated by monitoring the H/D exchange rate for the reconstituted exchanger. FTIR-ATR data reveal that 39% of the protein is α-helical, 20% β-sheets, 25% β-turns, and 16% random coils. H/D exchange measurements show that upon Ca^{2+} addition, a major tertiary conformational change occurs, characterized by an 11% reduction in solvent accessibility to the 120-kDa protein. On the contrary, when both XIP and Ca^{2+} were added, a 15% increase in solvent accessibility occurred. Interestingly, adding XIP alone resulted in no change in solvent accessibility. Likewise, in the presence of Ca^{2+}, XIP failed to affect the tertiary structure of the 70-kDa protein. The present data are compatible with an interaction model in which activator Ca^{2+} and inhibitory XIP interact at distinct binding sites, and where XIP binding requires the presence of Ca^{2+}.

EXPERIMENTAL PROCEDURES

Materials. All chemicals used were of the highest purity grade. HPLC water was used for the preparation of all solutions.

Preparation of Bovine Heart SLVs. Highly purified SLVs were isolated from bovine heart left ventricle as previously described (*28*, *29*) with minor modifications (*13*).

Purification and Reconstitution of the 120-kDa Na^+/Ca^{2+} Exchanger Protein. We have purified and reconstituted the 120-kDa Na^+/Ca^{2+} exchanger using a previously published protocol (*11*) except that SLVs were solubilized in a 20 mM (instead of 10 mM) decyl maltoside solution following alkaline extraction. Bio-beads SM-2 (Bio-Rad) were used for Triton X-100 removal to favor proteoliposome formation as described (*13*).

Gel Electrophoresis. A 12% (w/v) polyacrylamide Laemmli system was used (*30*). The sample buffer contained 10 mM NEM. Protein bands were revealed using Gelcode Blue stain reagent (Pierce), an enhanced Coomassie G-250 coloration solution. In brief, after electrophoresis, the gel was transferred to a clean tray and rinsed 3 times for 5 min with 200 mL of deionized water to remove SDS. Gelcode Blue stain (20 mL) was added, and the gel was incubated for 1 h, on a shaker. Finally, the staining reagent was discarded, and gel was washed in deionized water for 2 h with several changes of water. Kaleidoscope Prestained (Bio-Rad) standards were used for the molecular mass determination of protein bands.

Proteolysis. To determine the insertion mode of the reconstituted protein into the lipid vesicles (inside-out or right-side-out), intact reconstituted proteoliposomes were digested with Proteinase K (100 μg/mL) as previously described (*13*).

XIP Preparation and Modification. The XIP peptide (RRLLFYKYVYKRYRAGKQRG) was synthesized using the fluoren-9-ylmethoxycarbonyl strategy, as previously described (*31*). In some experiments, SNA-treated XIP was used [SNA acetylates lysine residues converting positively charged groups to neutral ones (*32*)]. A 30:1 mol/mol SNA/XIP mixture was incubated for 1 h at 37 °C at pH 9 (33 mM MOPS). The reaction was terminated by adding 13-fold excess of ethanolamine (mol/mol of SNA) (*33*). Before adding the XIP (modified or not) to the protein sample for H/D measurement, the modified XIP solution was run through a Sephadex G-15 column, preequilibrated in a 0.5 mM MOPS solution (pH 7.4), to eliminate SNA, ethanolamine, and residual ions.

Immunoblots. Proteins from SDS−PAGE were transferred to nitrocellulose at 220 mA (12 V) for 90 min in a semi-dry blotting apparatus (W.E.P. Co.). Nitrocellulose was then incubated with either "SWant" rabbit polyclonal antibody (SWant, Bellinzona, Switzerland) directed against the canine-purified Na^+/Ca^{2+} exchanger or "NCX1" rabbit polyclonal antibody (Eurogentec, Seraing, Belgium) directed against the peptide sequence aas 393−406, located in the large cytoplasmic domain of the bovine Na^+/Ca^{2+} exchanger (*13*). Immunoreactions were detected using sheep anti-rabbit IgG antibodies conjugated to alkaline phosphatase, as previously described (*13*).

Measurements of Na^+/Ca^{2+} Exchange Activity. Na^+/Ca^{2+} exchange activity in proteoliposomes was measured as Na_i^+-dependent $^{45}Ca_o^{2+}$ uptake using a previously described protocol (*11*). In some experiments, XIP (modified or not) was added to the Ca_o^{2+}-uptake medium, at a final concentration of 20 μM, to inhibit the Na^+/Ca^{2+} exchanger.

Secondary Structure Analysis by FTIR-ATR. Ten microliters of proteoliposome solution (containing 10−20 μg of purified exchanger protein) was layered on a germanium plate and dried by flushing with a nitrogen flux. The ATR plate was then sealed in a universal sample holder (Perkin-Elmer 186-0354). Sample on the ATR plate was deuterated by flushing a D_2O-saturated nitrogen stream for at least 2 h as previously described (*13*). The secondary structure composition of the protein was determined by the Fourier self-deconvolution method and a band-fitting procedure as described by Goormaghtigh et al. (*34*). Briefly, the self-deconvolution procedure allows the narrowing of the different secondary structure components overlapping within the amide I band region; then, the area under the bands obtained by self-deconvolution was quantified using least-squares iterative curve fitting of the Lorentzian line shapes in the spectral region between 1700 and 1600 cm^{-1}. This

fitting was performed on the amide I band before self-deconvolution to avoid artifacts due to the self-deconvolution procedure. Variations due to the sample hydration caused by the atmospheric water vapor content inside the spectrophotometer chamber were taken into account by subtracting from the sample spectrum a background spectrum recorded with the same germanium plate at the same position in the sample shuttle but in the absence of the protein sample for all conditions studied. In these conditions, the estimated standard deviation in the measurement of the secondary structure data compared to X-ray determination is 8.8% (*34*). The protein samples were analyzed in the absence of ligand (in 0.5 mM MOPS solution) and in the presence of Ca^{2+}, of Ca^{2+} and XIP, of Ca^{2+} and modified XIP, and of XIP alone. The Ca^{2+}:Na/Ca exchanger protein ratio was ~10:1 (mol/mol). The XIP:protein ratio was 1:20 w/w, corresponding to a ratio of ~2:1 mol/mol. At this ratio, XIP interference with infrared measurements is negligible.

Orientation of the Secondary Structure. Determination of peptide orientation by FTIR-ATR spectroscopy was performed as previously described (*35*).

Tertiary Structure Modification Analysis. Ten microliters of proteoliposome solution, containing 10−20 μg of purified protein, was prepared on a germanium plate as described under Secondary Structure Analysis by FTIR-ATR. The recording of the H/D exchange kinetics was carried out as previously described (*36*, *37*). In brief, the ATR plate containing the sample was sealed in a universal sample holder and flushed with a D_2O-saturated nitrogen flux by bubbling the nitrogen gas flow through five D_2O-containing vials. Bubbling was started at least 1 h before connecting the D_2O flux to the sample-containing sealed chamber. To ensure the stability of the measurement, 10 spectra were recorded before starting the exchange kinetics and were considered as the 0% deuteration value. The 100% deuteration value was obtained by extrapolation, assuming zero area under the amide II band. The validity of the amide II zero-area assumption has been demonstrated for denatured proteins (that completely exchange their hydrogen atoms) which are then renatured (*38*). At zero time, the D_2O flux was connected to the sealed chamber containing the sample. The geometry of the spectrophotometer shuttle allows one to run parallel recordings for two different H/D exchange experiments where a computerized program changed the shuttle position to follow both exchange kinetics. Typically, one sample placed on the shuttle was ligand-free while the other sample contained the ligand depending on the condition analyzed. Accordingly, a better reproducibility of the measurement was achieved when recordings for different conditions were obtained under identical conditions. Moreover, background exchange kinetics were carried out in the absence of sample using the same germanium plate placed at the same position in the shuttle and then subtracted from the sample-containing recorded kinetics. This allowed us to take into account unavoidable interference due to the atmospheric water vapor content inside the spectrophotometer chamber (*36*). Finally, the area of the amide II band was divided by the corresponding lipid ν(C═O) band area for each spectrum. This allowed us to take into account small variations due to spectral intensity decrease caused by swelling in the presence of the D_2O flux and also allowed us to avoid variations due to sample hydration, since the lipid ν(C═O) band is much less subject to modification caused by any H_2O traces present (*36*).

Table 1: Summary of Na^+/Ca^{2+} Exchange Activity Results[a]

protein	exchange sp act.	exchange sp act. after XIP addition	exchange sp act. after modified XIP addition
purified 120-kDa	525 ± 12 (n = 8)	6 ± 2 (n = 8)	489 ± 18 (n = 8)
purified 70-kDa	1075 ± 47 (n = 8)	1015 ± 33 (n = 4)	1041 ± 41 (n = 8)

[a] Exchange activities are shown for purified and reconstituted 120- and 70-kDa exchanger (15 μg). Na_i^+-dependent Ca_o^{2+} uptake was initiated by incubating 5 μL of Na^+-loaded vesicles in Ca^{2+}-uptake medium containing 0 mM Na^+. Blanks were obtained by incubating the vesicles in Ca^{2+}-uptake medium containing 140 mM Na^+. Background values were measured for 0 and 140 mM Na^+ solutions in the absence of vesicles and were subtracted to yield the results shown. Values are the means ± SEM. Exchange specific activity was computed in nanomoles of Ca^{2+} per second per milligram of protein. XIP, modified or not (see Experimental Procedures), was added to the uptake medium at a final concentration of 20 μM.

Different ligands tested in H/D exchange experiments were the same as described under Secondary Structure Analysis by FTIR-ATR.

Miscellaneous. Protein concentration was measured by the method of Schaffner and Weissmann (*39*) as modified by Newman et al. (*40*). The lipid content of samples was determined by measurement of choline content with an enzymatic phospholipid colorimetric test (Boehringer Mannheim).

Statistics and Calculations. All data are presented as mean ± SEM.

RESULTS

Purification and Reconstitution of the Bovine Heart Na^+/Ca^{2+} Exchanger. The Na^+/Ca^{2+} exchange specific activity in the Na^+/Ca^{2+} exchanger proteoliposomes was 525 ± 12 (n = 8) nmol at 40 μM Ca^{2+}, compared to an exchange activity of 18 ± 1 (n = 8) nmol of Ca^{2+} (mg of proteins)$^{-1}$ s^{-1} in control reconstituted SLVs (Table 1). The purification factor was 29. A lipid:protein ratio of ~7:1 (w/w) was used for reconstitution, yielding a single population of vesicles (*13*), the reconstituted proteins having the same orientation in all vesicles (see proteolysis experiment below).

Gel Electrophoresis and Immunoblots. Figure 1A shows SDS−PAGE gels at different purification steps under non-reducing conditions. A major band migrating at 120 kDa for the purified and reconstituted protein fraction was detected (lane 5). Moreover, an immunoblot was carried out using "SWant" antibody for protein fractions obtained in each purification step. The results show a major band at 120 kDa and a minor one at 160 kDa, throughout the whole purification procedure (Figure 1B).

Proteolysis of Intact Reconstituted Purified Na^+/Ca^{2+} Exchanger. The Ca^{2+} secondary regulation site and the XIP binding site are located in the large cytoplasmic loop of the Na^+/Ca^{2+} exchanger (*23*, *26*, *41*). Thus, to ensure that the purified and reconstituted Na^+/Ca^{2+} exchanger was inserted into lipid vesicles in a homogeneous way with an inside-out configuration, namely, with the regulatory binding sites located outside the liposomes and accessible for Ca^{2+} and XIP binding, we digested reconstituted proteoliposomes with Proteinase K and then carried out an immunoblot using

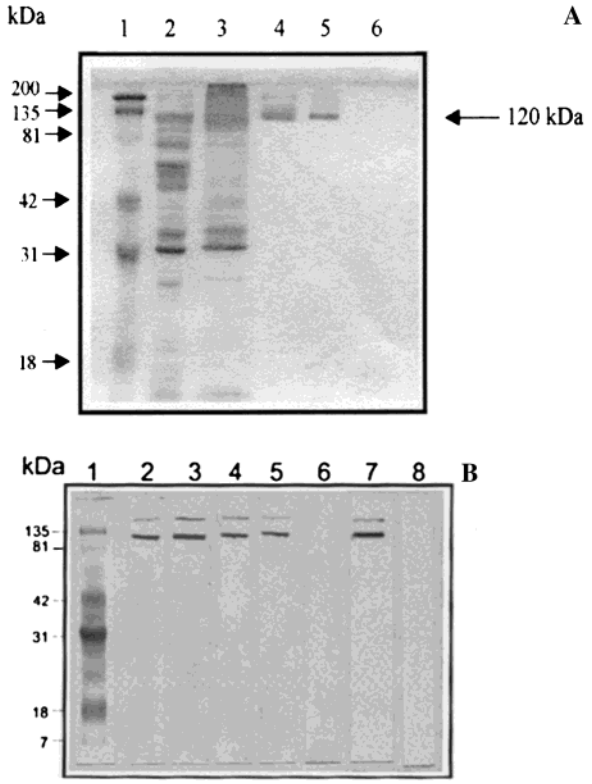

FIGURE 1: (A) Characterization of the 120-kDa Na^+/Ca^{2+} exchanger at the different purification steps. The starting material was 4 mg of SLV preparation (see Experimental Procedures for details). A 12% SDS−PAGE gel was used; proteins were revealed using Coomassie blue coloration as described under Experimental Procedures. Lane 1, molecular mass standard proteins (10 μL); lane 2, control reconstituted native SLVs (10 μg); lane 3, sample after alkaline extraction (10 μg); lane 4, sample after alkaline extraction and DEAE chromatography (~5 μg); lane 5, sample after alkaline extraction, DEAE, and WGA chromatography (~5 μg); lane 6, control protein-free asolectin vesicles. Protein samples were solubilized in sample buffer containing 10 mM NEM before loading into lanes. (B) Immunoblot carried out in parallel to the SDS−PAGE gel shown in (A). Lanes 1−6: same conditions as (A), and the immunoreaction was done using "SWant" antibody (dilution: 1:2000) as described under Experimental Procedures. Lane 7: immunoreaction of purified and reconstituted 120-kDa exchanger (~5 μg) with "NCX1" antibody (dilution: 1:1500). Lane 8: immunoreaction of digested purified and reconstituted exchanger protein (~5 μg) with "NCX1" antibody (1:1500) as described in "Proteolysis" under Experimental Procedures. Protein samples were solubilized in sample buffer containing 10 mM NEM before loading into lanes.

"NCX1" antibody (*13*). The "NCX1" antibody recognizes an intracytoplasmic epitope (aas 393−406) in the large hydrophilic domain between segments 5 and 6 of the Na^+/Ca^{2+} exchanger (*14*, *18*, *19*, *42*). Digestion of intact proteoliposomes with Proteinase K would yield a polypeptide with an approximate molecular mass of at least 60 kDa containing the "NCX1" epitope, if the purified protein is inserted in the normal mode (inside-in), or no such fragment, if the insertion mode is inside-out. Immunoblots with "NCX1" of digested proteoliposomes showed no positive reaction, indicating that we had a homogeneous population of inside-out reconstituted vesicles (Figure 1B, lane 7). As a control experiment, we incubated intact proteoliposomes with the supernatant collected after the second wash of digested proteoliposomes. Immunoreaction of "NCX1" antibody with this control sample was the same as for intact vesicles,

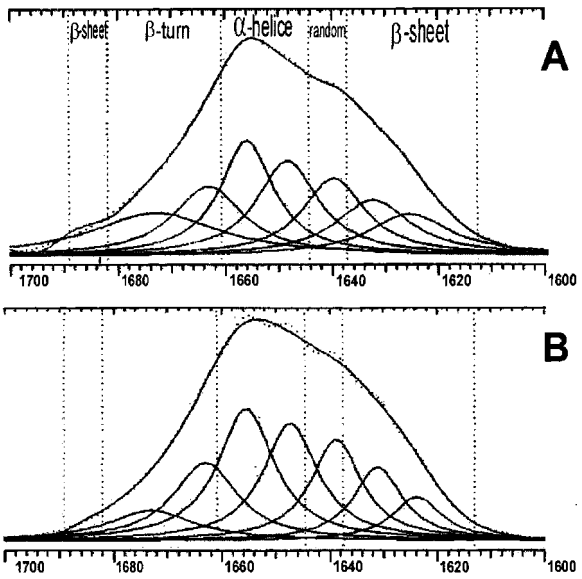

FIGURE 2: Analysis of the shape of the amide I absorption band in the spectrum of the reconstituted 120-kDa Na^+/Ca^{2+} exchanger. Spectra were recorded in the absence of ligand (panel A) and in the presence of both Ca^{2+} and XIP (panel B). Analysis of amide I band shape was carried out as previously described (*35*). Typical absorbency regions of the secondary structures of different peptide chains are 1646−1661 cm^{-1} (α-helices), 1615−1637 and 1682−1698 cm^{-1} (β-sheets), 1661−1681 cm^{-1} (β-turns), and 1637−1645 cm^{-1} (random coil).

demonstrating that the Proteinase K was completely eliminated before gel electrophoresis and immunoblot (Figure 1B, lane 8).

Secondary Structure Analysis of the 120-kDa Reconstituted Na^+/Ca^{2+} Exchanger. The lipid C═O band and the amide I band maximal absorptions were near 1737 and 1650 cm^{-1}, respectively, for spectra recorded in the different conditions used (see Experimental Procedures). The protein secondary structure was quantitatively evaluated by Fourier deconvolution and curve-fitting analysis of the amide I region for spectra recorded in the absence of ligand or in the presence of Ca^{2+}, XIP and Ca^{2+}, XIP alone, or Ca^{2+} with modified XIP, the latter peptide used as a control for XIP. At least three independent experiments were carried out for each condition. Figure 2 illustrates typical curve fitting of the amide I band showing different structural components (α-helices, β-sheets, β-turns, and random coils) of the Na^+/Ca^{2+} exchanger in ligand-free medium and in XIP- and Ca^{2+}-containing medium (panels A and B, respectively). In the absence of ligand, the secondary structure composition of the 120-kDa protein was 39% α-helices, 20% β-sheets, 25% β-turns, and 16% random coils and did not change significantly, within the expected 8.8% standard deviation (*34*), in the presence of different ligands tested (Table 2).

Orientation of the 120-kDa Na^+/Ca^{2+} Exchanger Protein Secondary Structure in the Lipid Membrane. The orientation of the reconstituted 120-kDa exchanger secondary structure was determined from FTIR-ATR spectra recorded with parallel and perpendicular polarized incident light, respectively (*35*). The dichroism spectrum (not shown) shows a maximal absorption at about 1659 cm^{-1} in the amide I region, characterizing an α-helix axis having a preferential orientation near the perpendicular to the lipid bilayer. This is in agreement with a topology model where α-helical trans-

Table 2: Secondary Structure Analysis of the 120-kDa Na^+/Ca^{2+} Exchanger in the Presence of Different Ligands Used[a]

120-kDa polypeptide	α-helices	β-sheets	β-turns	random
no ligand	39% (366 aas)	20% (188 aas)	25% (225 aas)	16% (150 aas)
XIP	37% (347 aas)	19% (178 aas)	25% (234 aas)	15% (141 aas)
Ca^{2+}+XIP	40% (375 aas)	18% (169 aas)	27% (253 aas)	15% (141 aas)
Ca^{2+}	41% (385 aas)	19% (178 aas)	26% (244 aas)	14% (131 aas)
Ca^{2+}+XIP-modified	40% (375 aas)	18% (169 aas)	26% (244 aas)	17% (159 aas)

[a] Percentage for α-helices, β-sheets, β-turns, and random structures was obtained by self-deconvolution of the amide I band from the spectrum of purified and reconstituted 120-kDa Na^+/Ca^{2+} exchanger under different conditions used. The total number of aas per secondary structure group was calculated on the basis that the cloned Na^+/Ca^{2+} exchanger yields 938 aas (*18*). The estimated standard deviation on the secondary structure composition is ~8.8% as described under Experimental Procedures.

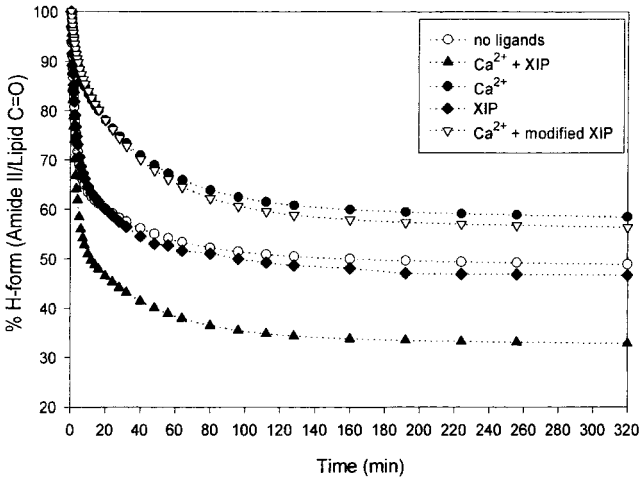

FIGURE 3: H/D exchange percentage computed as the amide II: lipid C═O ratio and reported as a function of time for the reconstituted 120-kDa Na^+/Ca^{2+} exchanger. Deuteration percentage was evaluated from the evolution of the amide II surface, as described under Experimental Procedures. For each curve, three independent experiments were carried out, and the average plot is shown. The dotted line for each curve represents the theoretical fit to the experimental data. The time scale is shown in minutes.

membrane segments and extramembranous α-helical structures have a preferential orientation perpendicular to lipid bilayer. No dichroism was detected for the β-sheet component in the spectrum.

Tertiary Structure Modification of the 120-kDa Polypeptide. It has been demonstrated that the proteoliposome drying procedure on ATR plates, as described under Experimental Procedures, does not alter the biochemical and biological properties of the proteins compared to the same proteins in native hydrated membranes. Indeed, protein samples dried on ATR plates retain their activity, like in native membranes, when resolubilized (*43*−*47*). Moreover, the gentle drying procedure we use does not allow the complete dehydration of the protein sample. The proteoliposome sample remains in a hydrated microenvironment after preparation on the ATR plate, as can been seen by the contribution of H_2O traces to the absorption peak at 3000 cm^{-1} (data not shown) (*47*). H/D exchange kinetic experiments were carried out in parallel in all combinations of studied conditions for the protein samples, i.e., with and without Ca^{2+}, with or without XIP, with Ca^{2+} and XIP, or with XIP alone, etc. The obtained H/D exchange spectra were recorded as a function of time (data not shown). For all conditions analyzed, the area under the amide II band was computed as described under Experimental Procedures and was plotted as the amide II: lipid ν(C═O) ratio as a function of time in minutes (Figure 3). Each experiment was independently repeated 3 times.

Table 3: Summary of H/D Exchange Rate Results for the 120-kDa Na^+/Ca^{2+} Exchanger[a]

substrate	α_1	α_2	α_3
no ligand	37% (347 aas)	14% (131 aas)	49% (460 aas)
Ca^{2+}	10% (94 aas)	30% (281 aas)	60% (563 aas)
Ca^{2+}+XIP	45% (422 aas)	21% (197 aas)	34% (319 aas)
XIP	35% (328 aas)	18% (169 aas)	47% (441 aas)
Ca^{2+}+XIP-modified	8% (75 aas)	31% (291 aas)	61% (572 aas)

[a] Percentage of amide hydrogen groups (α_1, α_2, and α_3) exchanging with deuterium and characterized by an average half-decay time of 2.5 s (T_1), 40 s (T_2), and 10^4 s (T_3), respectively. α_1, α_2, and α_3 are rapidly, intermediate, and slowly exchanging hydrogen families. Each percentage was computed by fitting the exchange curves shown in Figure 3. The total number of aas per hydrogen family was computed on the basis that the cloned bovine heart Na/Ca exchanger protein comprises 938 aas (*18*). The experimental standard deviation on the H/D measurements is of the order of 2−3% as previously discussed (*47*).

The H/D exchange is faster for protein sample prepared in the absence of ligand than for sample in the presence of Ca^{2+}. After 2 h, 51% of the amide protons (N−H) are exchanged compared to around 40%, respectively. This corresponds to an increased protection of approximately 103 aas. On the contrary, when Ca^{2+} and XIP are added, the exchange is faster (66%) than in the absence of ligand. Addition of XIP alone led to an exchange percentage similar to that in the absence of ligand condition (Table 3). To further demonstrate that the observed change in solvent accessibility induced by XIP in the presence of Ca^{2+} is XIP-specific and requires the presence of Ca^{2+}, namely, that it is not caused by nonspecific interactions between the peptide and the Na^+/Ca^{2+} exchanger protein that were altered by the addition of Ca^{2+}, we used as a control an SNA-modified XIP that fails to inhibit the Na^+/Ca^{2+} exchange activity, as discussed under Experimental Procedures and shown in Table 1. The SNA-modified XIP failed to induce any change in solvent accessibility in the absence Ca^{2+}, and in the presence of Ca^{2+}, the same conformation as with Ca^{2+} alone was obtained (Table 3). This means that the observed change induced by XIP is indeed specific and requires the presence of Ca^{2+}.

Considering that the H/D exchange rate is a first-order reaction, the exchange curve can be represented by a multiexponential decay function taking into account amide proton groups (α_i) exchanging at different rates, each characterized by a time period (T_i):

$$F(t) = \Sigma\alpha_i \exp(-t/T_i) \quad (1)$$

Three exponential terms characterized by a period, T_i, corresponding to a group of amide hydrogens, α_i (i = 1, 2, or 3), were chosen, corresponding to three families of exchanging protons (slow = α_1, intermediate = α_2, and fast-

exchanging = α_3) as previously described (*35*, *36*). The proportion of hydrogen atoms belonging to each family for different experimental conditions used is summarized in Table 3.

Secondary Structure Analysis of the 70-kDa Exchanger in the Presence of XIP. We have previously studied the secondary structure composition of the 70-kDa protein in the presence of Ca^{2+} (*35*). In the presence of XIP and Ca^{2+}, or XIP alone, the secondary structure composition of the 70-kDa protein was not modified (data not shown).

Hydrogen/Deuterium Exchange Study of the 70-kDa Polypeptide. Addition of XIP alone or both XIP and Ca^{2+} to the 70-kDa polypeptide did not lead to any tertiary structure change (data not shown) compared to the absence of ligand condition (*35*).

DISCUSSION

In this study, we purified and reconstituted an active 120-kDa Na^+/Ca^{2+} exchanger from bovine heart SLVs. The secondary structure of this protein was analyzed in the absence and in the presence of Ca^{2+}, an activator of the Na^+/Ca^{2+} exchanger (*21*, *22*), and XIP, a potent inhibitor of the exchanger (*23*, *25*, *26*). A modified XIP, having lost its inhibitory potential (*33*), was used as a control.

The secondary structure of the 120-kDa protein was composed of 39% α-helices, 20% *β*-sheets, 25% *β*-turns, and 16% random coils. The secondary structure composition was not significantly modified in the presence of Ca^{2+} and/or XIP, within the estimated standard deviation (8.8% as discussed under Experimental Procedures) (*34*) as reported in Table 2. The procedure described by Goormaghtigh et al. (*34*) for the secondary structure composition analysis yields a higher standard deviation than the 2.5% reached by Byler and Susi (*48*). However, the latter procedure uses a manual introduction of parameters for curve fitting and adjustment of the least-squares fitting parameters one at a time (*48*). The advantage of the procedure described by Goormaghtigh et al. (*34*) is that the fitting parameter input is completely automated, making the technique more objective and accessible to the investigator.

We have previously analyzed the secondary structure of the 70-kDa polypeptide (corresponding to the NH_2-terminal portion of the 120-kDa exchanger). If we subtract the number of aas belonging to each secondary structure class in the 70-kDa protein from those found in the 120-kDa protein, we obtain an extra 93 α-helical, 33 *β*-sheet, 126 *β*-turn, and 57 random structured aas (Table 4), corresponding to the COOH-terminal portion of the 120-kDa protein making ~318 aas and lacking in the 70-kDa polypeptide (*13*) (Figure 4). Assuming that membrane-spanning segments should be α-helical and contain 20 aas, our experimental data are in agreement with a membrane topology model having 4−6 α-helical transmembrane segments in the COOH-terminal portion of the 120-kDa exchanger, assuming a standard deviation of 8.8% on secondary structure composition values (Table 4). The hypothetical hydropathy profile-based membrane topology of the Na/Ca exchanger predicts 11 transmembrane segments, among which 6 are located in the COOH-terminal portion of the protein (*18*, *14*). However, a recent topology model based on mutational studies is rather in favor of 4 transmembrane segments in that portion of the protein (*19*).

Table 4: Comparison of the 120- and 70-kDa Na^{2+}/Ca^{2+} Exchanger Secondary Structures in the Absence of Ligand[a]

polypeptide	α-helices	*β*-sheets	*β*-turns	random coils
120-kDa	39% (366 ± 29)	20% (188 ± 15)	25% (225 ± 18)	16% (150 ± 12)
70-kDa	44% (273 ± 22)	25% (155 ± 12)	16% (99 ± 8)	15% (93 ± 7)
318 aas	29% (93 ± 36)	10% (33 ± 19)	40% (126 ± 17)	18% (57 ± 14)

[a] The secondary structure composition of the 70-kDa protein was reproduced from reference (*35*). Numbers in parentheses represent the number of aas belonging to each secondary structure group considering that the 120-kDa protein and the 70-kDa one comprise 938 and 620 aas, respectively. Values for the 70-kDa protein were reported from reference (*35*).

Another deduction resulting from the comparison between the secondary structures of the 70- and 120-kDa proteins is that the cytoplasmic loop and the transmembrane-joining loops of the 318 aa polypeptide have little α-helical content compared to the cytoplasmic loop of the 70-kDa polypeptide (*35*).

Because Ca^{2+} and/or XIP did not affect the secondary structure of the protein, the changes in H/D exchange rate induced by these ligands are indicative of changes in tertiary structure. In the absence of ligand, H/D exchange measurements showed that about 460 aas of the Na^+/Ca^{2+} exchanger belong to the α_3 fraction inaccessible to exchange (Table 3). If we subtract from this fraction the number of aas corresponding to transmembrane segments (Figure 4A) inaccessible to exchange, we find that ~280 additional aas do not exchange their hydrogen atoms. Inaccessibility to solvent of membrane-spanning regions of proteins was previously demonstrated for many membrane proteins (*49*−*51*). Accordingly, either more membrane-spanning segments are present than theoretically predicted and/or a portion of the extramembranous region is highly structured, accounting for solvent inaccessibility.

Moreover, in the absence of ligand, the number of aas belonging to the intermediate exchanging population of the 120-kDa protein (Table 3) was lower than that of the 70-kDa protein [131 and 155 aas, respectively, see ref (*35*)]. This indicates a difference in the secondary and/or tertiary structure of the NH_2 portion of the 70- and 120-kDa polypeptides.

Ca^{2+} binding to the 120-kDa Na^+/Ca^{2+} exchanger led to a shift of about 253 rapidly exchanging aas to the intermediate (150 aas) and slow (103 aas) exchanging population. In contrast, Ca^{2+} binding to the 70-kDa protein induced a predominant shift from the rapidly exchanging population (101 aas) to the slow (77 aas) instead of the intermediate exchanging population (*35*). This indicates that the protein folding process or the conformational change concerns different regions of the two proteins, at least partially. Hence, the COOH-terminal portion of the cytoplasmic loop is involved in the global conformational change. The Ca^{2+}-induced increase of protection of a relatively large number of aas can be interpreted in terms of a folding or "membrane penetration" of a protein portion, in relation to the two conformations (E_1 or E_2) acquired during the activity cycle or the intermediate conformations acquired during the Ca^{2+}-transport cycle (*9*, *10*). Similar tertiary structure changes have

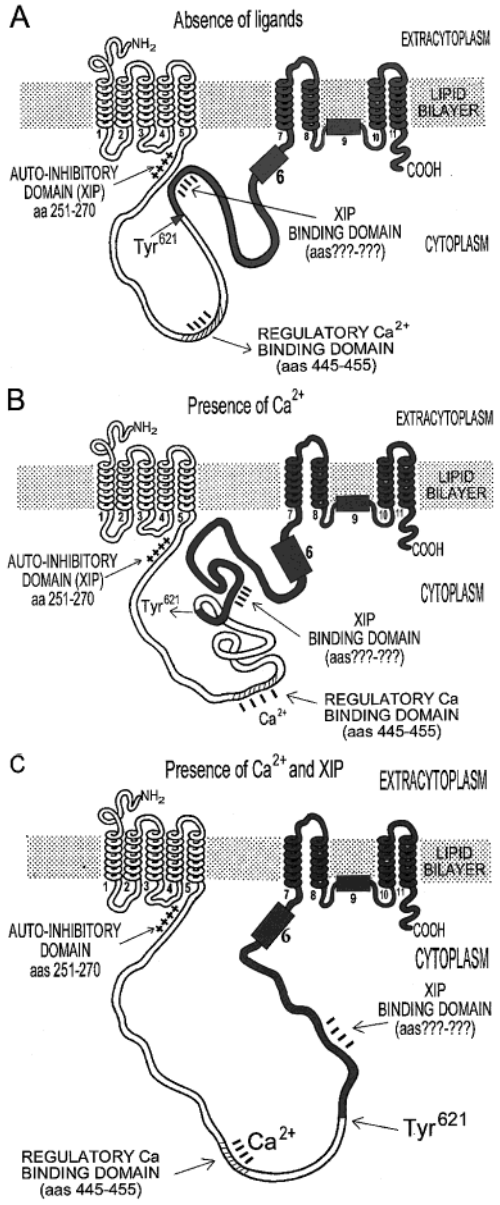

FIGURE 4: Drawing illustrating the conformational changes of the 120-kDa Na^+/Ca^{2+} exchanger induced by its regulators. This illustration is based on the new model, proposed by Nicoll et al. (*19*) and Iwamoto et al. (*20*). Transmembrane segments are shown as helices and numbered in boldface characters, except segments **6** and **9**, drawn as a box, to denote the possibility that they are not membrane-spanning, as proposed (*19*, *20*). The protein portion, shown in gray, is the **318** aa polypeptide corresponding to the COOH-terminal portion of the 120-kDa protein that is lacking in the 70-kDa one. The 70-kDa fragment is the NH_2-terminal portion of the 120-kDa protein and ends around Tyr^{621}, as indicated in the panels. Panel A: In the absence of ligand, the negatively charged domain (aas 445−455) binds the endogenous XIP domain (aas 251−270), thus preventing exogenous XIP binding. Panel B: Ca^{2+} binding to its regulatory site dislocates it from the auto-inhibitory region and induces an active protein conformation characterized by the folding of some secondary structures into a more compact configuration, making the XIP binding domain accessible to exogenous XIP. Panel C: When XIP is added in the presence of Ca^{2+}, an important conformational change occurs with opposite effect to that observed upon Ca^{2+} addition; i.e., the protein adopts an unfolded conformation leading to its inhibition. N.B.: The rearrangements of the intracellular loop illustrated in panels A, B, and C are solely indicative of changes in the *tertiary* structure of the protein and must not be taken either as changes in *secondary* structure or as the actual conformational changes that occur upon ligand binding.

been observed for other membrane proteins (*36*, *50*, *52*−*54*).

Interestingly, no tertiary structure changes were observed when XIP alone was added. When both XIP and Ca^{2+} were present, an increased solvent accessibility to 141 aas of the slowly exchanging hydrogen population occurred, in almost equal proportions to the intermediate (66 aas) and rapidly exchanging ones (75 aas). A similar conformational change was observed in the case of the P-glycoprotein upon MgATP addition (*50*). The evidence that the conformational change induced by XIP was specific and required the presence of Ca^{2+} was further confirmed by the observation that the SNA-modified XIP, that does not inhibit the Na^+/Ca^{2+} exchanger protein (Table 1), failed to induce any conformational changes in the absence of ligand and gave the same tertiary structure change as Ca^{2+} alone when added together. Since SNA neutralizes the lysines responsible for the specific inhibitory interaction of XIP with the Na^+/Ca^{2+} exchanger protein (*33*), our data indicate that the observed conformational change is due to a specific interaction between XIP and the exchanger protein and that the XIP interaction occurs only in the presence of Ca^{2+}.

In the 70-kDa exchanger, XIP addition, in the absence or the presence Ca^{2+}, induced no conformational changes (data not shown). This finding is consistent with $^{45}Ca^{2+}$ uptake measurements where XIP had no inhibitory effect (Table 1). An important implication of this absence of inhibition is that the COOH-terminal, rather than the NH_2-terminal, portion of the intracytoplasmic loop is involved in inhibition by XIP. This was previously suggested by Matsuoka et al. (*23*), who observed no regulation of the exchanger by XIP following deletion mutagenesis of aas 562−685 or chymotrypsin treatment. The latter treatment shifts the Na/Ca exchanger from the 120-kDa to the 70-kDa form (*11*). Using XIP-affinity column chromatography and an XIP cross-linking probe, Hale et al. showed that XIP binds to a negatively charged region of the NH_2-terminal portion of the cytoplasmic loop (IDDDIFEEDEN; aas 445−455) (*26*). However, their data do not exclude that XIP may interact with another region(s) of the loop between aas 562 and 685 that failed to purify by affinity column chromatography or was (were) proteolytically degraded. Likewise, it is unclear in the latter study to what extent the cysXIP probe used in cross-linking experiments binds the native protein and inhibits Na^+/Ca^{2+} exchange.

Incidentally, the fact that XIP "suppressed" or "antagonized" the conformational change induced by Ca^{2+} indicates that the later change concerns a portion of the protein involved in the regulation by Ca^{2+} rather than a region involved in the transport of the ion.

The conformational changes induced by Ca^{2+} activation and XIP inhibition of the Na^+/Ca^{2+} exchanger can be summarized as follows: in the absence of ligand, the endogenous XIP domain (aas 251−270) binds to the large cytoplasmic loop (*25*, *55*, *56*) which inactivates the exchanger (Figure 4A). Ca^{2+} binding to its regulatory site (aas 445−455) leads to the dissociation of the endogenous XIP domain from its binding site (Figure 4B) and to a tertiary structure change making the protein more compact. At this stage, XIP addition gives an unfolded conformation inhibiting Na^+/Ca^{2+} exchange activity (Figure 4C). This increased accessibility should not be necessarily interpreted as resulting from the

formation or the opening of a pore-like structure in the protein, considering that the cytoplasmic loop makes ~500 aas and is located at the extravesicular part. Thus, binding of exogenous XIP peptide might destabilize this large loop, leading to an increased accessibility. Accordingly, the tertiary conformational change of the 120-kDa protein, when inhibited by exogenous XIP, is different from that observed in the absence of ligand, namely, when the protein is in its auto-inhibited state. This is not surprising since the XIP peptide, when externally added, binds to the cytoplasmic loop and prevents the endogenous XIP domain from inducing the auto-inhibited conformation (*25*, *55*, *56*).

XIP has no effect in the absence of Ca^{2+} probably because the XIP binding site is not accessible in the auto-inhibited state (Figure 4A). Thus, Ca^{2+} binding exposes or structurally modifies the XIP binding site to allow exogenous XIP binding. Consequently, XIP binding does not simply depend on electrostatic interactions between opposite charges, but also involves structural parameters. It follows that XIP and Ca^{2+} binding to the protein occurs at different sites in a noncompetitive manner, Ca^{2+} promoting XIP binding (*23*, *57*).

Infrared dichroism results show the presence of α-helices having a transmembrane orientation perpendicular to the lipid bilayer. The other secondary structures did not show any significant orientation. This is in agreement with a topology model where α-helical transmembrane segments and extramembranous ordered α-helical structures have a preferential orientation perpendicular to the lipid bilayer.

In conclusion, the secondary structure of the 120-kDa protein is composed of 39% α-helices, 20% β-sheets, 25% β-turns, and 16% random coils. Comparison of the secondary structures of the 120- and 70-kDa polypeptides shows that the COOH-terminal portion of the intracellular loop has little α-helical structure, in contrast with the NH_2-terminal portion. Ca^{2+} addition induces the shielding of ~103 aas in the 120-kDa protein, like in the 70-kDa protein; but, the observed change concerned different parts of the two proteins. XIP addition in the presence of Ca^{2+} induced an unfolded conformation larger than that seen in the absence of ligand. No such effects were observed for the 70-kDa protein, suggesting that XIP inhibition involves the COOH-terminal region of the cytoplasmic loop. Finally, XIP had no effect in the absence of Ca^{2+}, indicating that XIP binding has conformational requirements fulfilled by Ca^{2+} binding, and that XIP and Ca^{2+} bind separate sites.

REFERENCES

1. Callewaert, G. (1992) *Cardiovasc. Res. 26*, 923−932.
2. Barry, W. H., and Bridge, J. H. (1993) *Circulation 87*, 1806−1815.
3. Maxwell, K., Scott, J., Omelchenko, A., Lukas, A., Lu, L., Lu, Y., Hnatowich, M., Philipson, K. D., and Hryshko, L. V. (1999) *Am. J. Physiol. 277*, H2212−H2221.
4. Terracciano, C. M., Souza, A. I., Philipson, K. D., and MacLeod, K. T. (1998) *J. Physiol. (London) 512 (Pt. 3)*, 651−667.
5. Eisner, D. A., and Lederer, W. J. (1985) *Am. J. Physiol. 248*, C189−C202.
6. Hilgemann, D. W., Collins, A., Cash, D. P., and Nagel, G. A. (1991) *Ann. N.Y. Acad. Sci. 639*, 126−139.
7. Khananshvili, D. (1990) *Biochemistry 29*, 2437−2442.
8. Khananshvili, D. (1991) *Ann. N.Y. Acad. Sci. 639*, 85−95.
9. Khananshvili, D., Shaulov, G., and Weil-Maslansky, E. (1995) *Biochemistry 34*, 10290−10297.
10. Khananshvili, D., Weil-Maslansky, E., and Baazov, D. (1996) *Ann. N.Y. Acad. Sci. 779*, 217−235.
11. Philipson, K. D., Longoni, S., and Ward, R. (1988) *Biochim. Biophys. Acta 945*, 298−306.
12. Durkin, J. T., Ahrens, D. C., Pan, Y. C., and Reeves, J. P. (1991) *Arch. Biochem. Biophys. 290*, 369−375.
13. Saba, R. I., Bollen, A., and Herchuelz, A. (1999) *Biochem. J. 338 (Pt. 1)*, 139−145.
14. Nicoll, D. A., Longoni, S., and Philipson, K. D. (1990) *Science 250*, 562−565.
15. Nicoll, D. A., Quednau, B. D., Qui, Z., Xia, Y. R., Lusis, A. J., and Philipson, K. D. (1996) *J. Biol. Chem. 271*, 24914−24921.
16. Li, Z., Matsuoka, S., Hryshko, L. V., Nicoll, D. A., Bersohn, M. M., Burke, E. P., Lifton, R. P., and Philipson, K. D. (1994) *J. Biol. Chem. 269*, 17434−17439.
17. Kofuji, P., Lederer, W. J., and Schulze, D. H. (1994) *J. Biol. Chem. 269*, 5145−5149.
18. Aceto, J. F., Condrescu, M., Kroupis, C., Nelson, H., Nelson, N., Nicoll, D., Philipson, K. D., and Reeves, J. P. (1992) *Arch. Biochem. Biophys. 298*, 553−560.
19. Nicoll, D. A., Ottolia, M., Lu, L., Lu, Y., and Philipson, K. D. (1999) *J. Biol. Chem. 274*, 910−917.
20. Iwamoto, T., Nakamura, T. Y., Pan, Y., Uehara, A., Imanaga, I., and Shigekawa, M. (1999) *FEBS Lett. 446*, 264−268.
21. DiPolo, R. (1979) *J. Gen. Physiol. 73*, 91−113.
22. DiPolo, R., and Beauge, L. (1987) *J. Gen. Physiol. 90*, 505−525.
23. Matsuoka, S., Nicoll, D. A., Reilly, R. F., Hilgemann, D. W., and Philipson, K. D. (1993) *Proc. Natl. Acad. Sci. U.S.A. 90*, 3870−3874.
24. Levitsky, D. O., Nicoll, D. A., and Philipson, K. D. (1994) *J. Biol. Chem. 269*, 22847−22852.
25. Li, Z., Nicoll, D. A., Collins, A., Hilgemann, D. W., Filoteo, A. G., Penniston, J. T., Weiss, J. N., Tomich, J. M., and Philipson, K. D. (1991) *J. Biol. Chem. 266*, 1014−1020.
26. Hale, C. C., Bliler, S., Quinn, T. P., and Peletskaya, E. N. (1997) *Biochem. Biophys. Res. Commun. 236*, 113−117.
27. Gall, D., and Susa, I. (1999) *Biophys. J. 77*, 45−53.
28. Philipson, K. D., and Ward, R. (1987) *Biochim. Biophys. Acta 897*, 152−158.
29. Cheon, J., and Reeves, J. P. (1988) *J. Biol. Chem. 263*, 2309−2315.
30. Laemmli, U. K. (1970) *Nature 227*, 680−685.
31. Van Eylen, F., Svoboda, M., and Herchuelz, A. (1997) *Cell Calcium 21*, 185−193.
32. Creighton, T. E. (1984) *Methods Enzymol. 107*, 305−329.
33. Xu, W., Denison, H., Hale, C. C., Gatto, C., and Milanick, M. A. (1997) *Arch. Biochem. Biophys. 341*, 273−279.
34. Goormaghtigh, E., Cabiaux, V., and Ruysschaert, J. M. (1990) *Eur. J. Biochem. 193*, 409−420.
35. Saba, R. I., Ruysschaert, J. M., Herchuelz, A., and Goormaghtigh, E. (1999) *J. Biol. Chem. 274*, 15510−15518.
36. Goormaghtigh, E., Vigneron, L., Scarborough, G. A., and Ruysschaert, J. M. (1994) *J. Biol. Chem. 269*, 27409−27413.
37. Goormaghtigh, E., Cabiaux, V., and Ruysschaert, J. M. (1994) *Subcell. Biochem. 23*, 405−450.
38. de Jongh, H. H., Goormaghtigh, E., and Ruysschaert, J. M. (1997) *Biochemistry 36*, 13603−13610.
39. Schaffner, W., and Weissmann, C. (1973) *Anal. Biochem. 56*, 502−514.
40. Newman, M. J., Foster, D. L., Wilson, T. H., and Kaback, H. R. (1981) *J. Biol. Chem. 256*, 11804−11808.
41. Kleiboeker, S. B., Milanick, M. A., and Hale, C. C. (1992) *J. Biol. Chem. 267*, 17836−17841.
42. Porzig, H., Li, Z., Nicoll, D. A., and Philipson, K. D. (1993) *Am. J. Physiol. 265*, C748−C756.
43. Goormaghtigh, E., Vigneron, L., Scarborough, G. A., and Ruysschaert, J. M. (1994) *J. Biol. Chem. 269*, 27409−27413.
44. Goormaghtigh, E., Cabiaux, V., and Ruysschaert, J. M. (1994) *Subcell. Biochem. 23*, 405−450.

45. Goormaghtigh, E., Cabiaux, V., and Ruysschaert, J. M. (1994) *Subcell. Biochem. 23*, 363−403.
46. Goormaghtigh, E., Cabiaux, V., and Ruysschaert, J. M. (1994) *Subcell. Biochem. 23*, 329−362.
47. Goormaghtigh, E., Raussens, V., and Ruysschaert, J. M. (1999) *Biochim. Biophys. Acta 1422*, 105−185.
48. Byler, D. M., and Susi, H. (1986) *Biopolymers 25*, 469−487.
49. Challou, N., Goormaghtigh, E., Cabiaux, V., Conrath, K., and Ruysschaert, J. M. (1994) *Biochemistry 33*, 6902−6910.
50. Sonveaux, N., Shapiro, A. B., Goormaghtigh, E., Ling, V., and Ruysschaert, J. M. (1996) *J. Biol. Chem. 271*, 24617−24624.
51. Raussens, V., Ruysschaert, J. M., and Goormaghtigh, E. (1997) *J. Biol. Chem. 272*, 262−270.
52. Shapiro, A. B., and Ling, V. (1994) *J. Biol. Chem. 269*, 3745−3754.
53. Addison, R., and Scarborough, G. A. (1982) *J. Biol. Chem. 257*, 10421−10426.
54. Barth, A., Kreutz, W., and Mantele, W. (1997) *J. Biol. Chem. 272*, 25507−25510.
55. Kleiboeker, S. B., Milanick, M. A., and Hale, C. C. (1992) *J. Biol. Chem. 267*, 17836−17841.
56. He, Z., Feng, S., Tong, Q., Hilgemann, D. W., and Philipson, K. D. (2000) *Am. J. Physiol. 278*, C661−C666.
57. He, Z., Petesch, N., Voges, K., Roben, W., and Philipson, K. D. (1997) *J. Membr. Biol. 156*, 149−156.

BI0010672